

## Thermoelectric properties of HfN/ScN metal/semiconductor superlattices: a first-principles study

This content has been downloaded from IOPscience. Please scroll down to see the full text.

2012 J. Phys.: Condens. Matter 24 415303

(<http://iopscience.iop.org/0953-8984/24/41/415303>)

View [the table of contents for this issue](#), or go to the [journal homepage](#) for more

Download details:

IP Address: 136.152.38.197

This content was downloaded on 09/02/2015 at 20:07

Please note that [terms and conditions apply](#).

# Thermoelectric properties of HfN/ScN metal/semiconductor superlattices: a first-principles study

Bivas Saha<sup>1,2</sup>, Timothy D Sands<sup>1,2,3</sup> and Umesh V Waghmare<sup>4</sup>

<sup>1</sup> School of Materials Engineering, Purdue University, West Lafayette, IN 47907, USA

<sup>2</sup> Birck Nanotechnology Center, Purdue University, West Lafayette, IN 47907, USA

<sup>3</sup> School of Electrical and Computer Engineering, Purdue University, West Lafayette, IN 47907, USA

<sup>4</sup> Theoretical Sciences Unit, Jawaharlal Nehru Centre for Advanced Scientific Research, Jakkur, Bangalore 560064, India

E-mail: [bsaha@purdue.edu](mailto:bsaha@purdue.edu)

Received 26 June 2012, in final form 6 September 2012

Published 26 September 2012

Online at [stacks.iop.org/JPhysCM/24/415303](http://stacks.iop.org/JPhysCM/24/415303)

## Abstract

Nitride-based metal/semiconductor superlattices are promising candidates for high-temperature thermoelectric applications. Motivated by recent experimental studies, we perform first-principles density functional theory based analysis of electronic structure, vibrational spectra and transport properties of HfN/ScN metal/semiconductor superlattices for their potential applications in thermoelectric and thermionic energy conversion devices. Our results suggest (a) an asymmetric linearly increasing density of states and (b) flattening of conduction bands along the cross-plane  $\Gamma$ -Z direction near the Fermi energy of these superlattices, as is desirable for a large power factor. The n-type Schottky barrier height of 0.13 eV at the metal/semiconductor interface is estimated by the microscopic averaging technique of the electrostatic potential. Vibrational spectra of these superlattices show softening of transverse acoustic phonon modes and localization of ScN phonons in the vibrational energy gap between the HfN (metal) and ScN (semiconductor) states. Our estimates of lattice thermal conductivity within the Boltzmann transport theory suggests up to two orders of magnitude reduction in the cross-plane lattice thermal conductivity of these superlattices compared to their individual bulk components.

(Some figures may appear in colour only in the online journal)

## 1. Introduction

Thermoelectric materials that convert heat flux directly into electrical power have great promise in dealing with present day energy challenges [1–3]. Devices made with them are robust, environmentally friendly and possess no movable parts. The efficiency of these materials is represented by the dimensionless figure of merit  $ZT = \frac{S^2\sigma T}{\kappa}$ , where  $S$  is the Seebeck coefficient,  $\sigma$  is the electrical conductivity,  $\kappa$  is the thermal conductivity and  $T$  is the temperature, respectively. To be competitive with conventional power generation and refrigeration technologies, we need materials with  $ZT$  of at least 3 over a wide temperature range. A good thermoelectric material must have high electrical conductivity to minimize Joule heating, low thermal conductivity to prevent thermal

shorting and a large Seebeck coefficient to convert waste heat flux into electricity or electrical power to cooling. However, research in the past fifty years with conventional materials such as Bi<sub>2</sub>Te<sub>3</sub> and PbTe [4, 5] has yielded  $ZT$  values in the range of 1–1.5. Achieving  $ZT > 2$  is difficult because of mutually conflicting parameters in the  $ZT$  expression. Pioneering theoretical works of Dresselhaus and Hicks [6, 7] have suggested that nanostructured materials should have a higher thermoelectric efficiency due to the quantum confinement of the electrons and scattering of phonons at surfaces and interfaces. Subsequent experimental work demonstrated  $ZT$  enhancement in nanostructured materials [8, 9], but a full understanding of the mechanism in enhancement has not yet been achieved.

Mahan *et al* [10, 11] first suggested that the efficiency of thermoelectric materials can be enhanced by thermionic emission of electrons over the Schottky barriers between metal and semiconductors in multilayers and superlattices. Shakouri *et al* [12–15] later pointed out that highly degenerate semiconductors and metal-based superlattices could achieve a thermoelectric power factor exceeding bulk values. The central ideas for increasing the thermoelectric figure of merit in multilayers and superlattices are (1) to control the Schottky barrier height for efficient energy filtering of electrons during transport, thereby enhancing the Seebeck coefficient while retaining a high electrical conductivity, and (2) to use the interface between the component materials as a phonon filter, thereby reducing the cross-plane lattice thermal conductivity. Understanding the nature of the metal/semiconductor interfaces is also crucial in designing multilayers or superlattices with high  $ZT$ .

In this work, we present first-principles density functional theory based calculations of electronic structure and vibrational spectra, as a foundation for developing an understanding of the temperature-dependent cross-plane transport properties of HfN/ScN metal/semiconductor superlattices. Early transition metal nitrides such as HfN and ScN crystallize in the rocksalt structure, with an octahedral bonding configuration. These phases are hard, chemically stable, possess high corrosion resistance, and have extremely high melting temperatures. In our previous studies on bulk nitrides [16, 17], we have shown that ScN is semiconducting in nature with an indirect  $\Gamma$ -X band gap of 0.89 eV, while HfN shows metallic behaviour. We have also analysed the thermoelectric properties of the related ZrN/ScN metal/semiconductor superlattice system [18, 19] in previous work, where it was demonstrated that Schottky barrier formation in the metal/semiconductor interface gives rise to the flat localized states near the Fermi energy which contribute to an enhanced power factor. The lattice thermal conductivity of the superlattices was also found to be smaller than the component bulk materials by a factor of 10–100. The replacement of ZrN with HfN is motivated by the fact that the mismatch in the bulk phonon densities of states between HfN and ScN is much larger than that of ZrN and ScN (details of which are presented in our bulk nitride analysis [16]), which in turn should suppress the lattice thermal conductivity of HfN/ScN-based superlattices to a greater degree than ZrN/ScN superlattices. Another important advantage of using HfN is that it is closely lattice-matched with ScN (both HfN and ScN have a lattice constant of 4.52 Å), whereas in ZrN/ScN superlattices, the lattice mismatch is 1.5%.

## 2. Methods of calculations

We use the plane wave self-consistent field (PWSCF) implementation of the density functional theory with a generalized gradient approximation (GGA) [20] to the exchange correlation energy and ultrasoft pseudopotentials [21] to represent the interaction between ionic cores and valence electrons. Plane wave (PW) basis sets with energy cutoffs of 30 and 180 Ryd were used to represent

the electronic wavefunction and charge density respectively. Integration over the Brillouin zone is carried out using the Monkhorst–Pack [22] scheme with a  $10 \times 10 \times 10/n$  mesh of  $k$ -points for  $n/n$  superlattice, and occupation numbers are smeared using the Methfessel–Paxton [23] scheme with a broadening of 0.003 Ryd. A Hubbard  $U$  correction [24], with  $U = 3.5$  eV, is included along with GGA for Sc atoms to correctly describe the electronic bandwidth and gap. (See details and validity of our methods used in extensive analysis of bulk properties of ScN, ZrN, and HfN in [16].)

Phonon spectra and densities of states are determined accurately within the framework of self-consistent density functional perturbation theory [25], with plane wave basis of energy cutoffs of 40 Ryd and 750 Ryd to describe the wavefunction and charge density respectively. In order to understand the detailed features of phonon spectra, force constant matrices were obtained on a  $3 \times 3 \times 1$  (for  $2/2$  superlattice)  $q$ -point mesh. The dynamical matrices at arbitrary wavevectors were then obtained through Fourier transform based interpolation.

The electrical conductivity ( $\sigma$ ) and the Seebeck coefficient ( $S$ ) are calculated within the Boltzmann transport theory under the relaxation time approximation, and are given by the expression [26]

$$\sigma_{\alpha\beta} = e^2 \int_{-\infty}^{\infty} \sum_k v_{\alpha}(k) v_{\beta}(k) \tau(k) \delta(\varepsilon - \varepsilon(k)) \left( -\frac{\delta f_0}{\delta \varepsilon} \right) d\varepsilon$$

$$S_{\alpha\beta} = \frac{e}{T\sigma} \int_{-\infty}^{\infty} \sum_k v_{\alpha}(k) v_{\beta}(k) \tau(k) \delta(\varepsilon - \varepsilon(k)) (\varepsilon - \mu) \left( -\frac{\delta f_0}{\delta \varepsilon} \right) d\varepsilon,$$

where  $v_{\alpha}(k)$  and  $v_{\beta}(k)$  are the group velocities of electrons in the  $\alpha$  and  $\beta$  directions respectively,  $\delta(\varepsilon - \varepsilon(k))$  is the density of electronic states,  $\tau(k)$  is the relaxation time,  $\mu$  is the chemical potential and  $f_0$  is the Fermi–Dirac distribution function. Eigenenergies of the electron are calculated on a very dense mesh of  $k$ -points in the entire Brillouin zone, and subsequently used to estimate the group velocities.

It is not simple to estimate the electronic relaxation time from first principles, and we do not have the knowledge of  $\tau(k)$  for the bulk materials (HfN, ScN) or HfN/ScN superlattices. To the best of our knowledge there are no experimental estimates of  $\tau(k)$  mentioned in the literature for any of these materials. Hence we assume that the electronic relaxation time is independent of electron energy and the same for all of the materials; hence, the electronic relaxation time is removed from the integral, and the focus is on the relative behaviour of the calculated electrical conductivity and Seebeck coefficient. This is an oversimplification, but could reveal meaningful trends in electronic contributions to transport properties of these superlattices.

The lattice thermal conductivity  $\kappa_{\alpha\beta}$  (i.e along  $\alpha\beta$  direction) is obtained within Boltzmann theory

$$\kappa_{\alpha\beta} = \hbar \sum_{\lambda} \int \frac{d^3q}{(2\pi)^3} v_{\alpha\lambda}(q) v_{\beta\lambda}(q) \omega_{\lambda}(q) \tau_{\lambda}(q) \times \left[ \frac{dn_{\text{B}}[\omega_{\lambda}(q)]}{dT} \right],$$

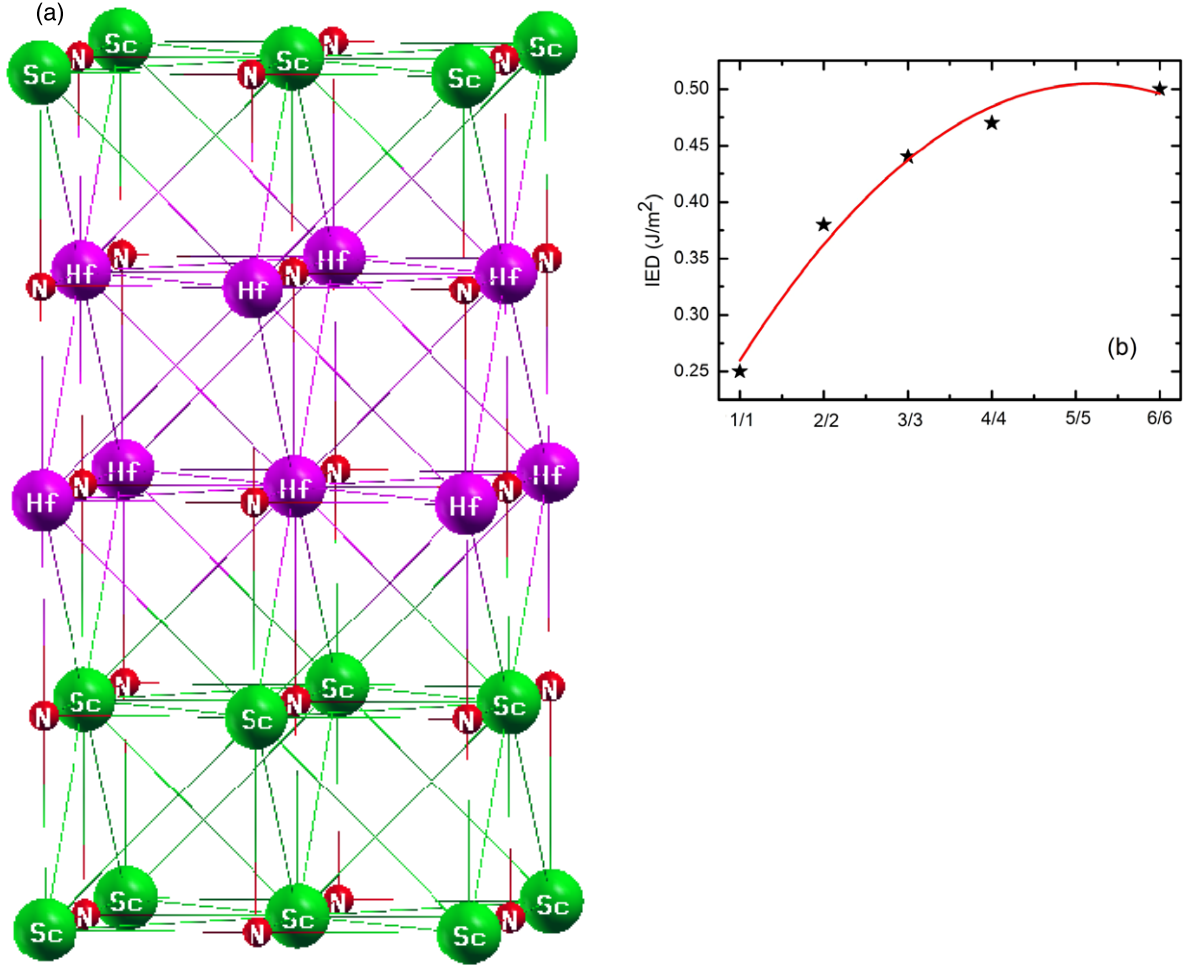


**Figure 1.** (a) Schematic description of a 2/2 HfN/ScN crystal structure. (b) Interface energy density (IED) of HfN/ScN superlattices as a function of their period. The IED is seen to be converging rapidly as we increase the period. (The solid line acts as a guide to eye to represent the convergence of the IED.)

where  $\lambda$  is the polarization vector of the normal mode,  $v_{\alpha\lambda}(q)$  and  $v_{\beta\lambda}(q)$  are the group velocities of phonons along  $\alpha$  and  $\beta$  directions respectively,  $\tau_{\lambda}(q)$  is the relaxation time, and  $n_{\text{B}}[\omega_{\lambda}(q)]$  is the Bose–Einstein distribution function. The relaxation time  $\tau_{\lambda}(q)$  is assumed to be constant and kept outside the integral. Eigenfrequencies were obtained on a dense mesh of 1000  $k$ -points over the entire Brillouin zone, which were subsequently used in determination of  $v_{\alpha\lambda}(q)$  and  $v_{\beta\lambda}(q)$ .

### 3. Results

#### 3.1. Structural details

HfN( $m$ )/ScN( $n$ ) superlattices are grown by stacking  $m$ -layers of metal (HfN) and  $n$ -layers of semiconductor (ScN) repetitively. Both the in-plane and the cross-plane lattice constant are optimized and the structures are fully relaxed until the forces on each atom are less than 0.001 Ryd/Bohr (crystal structure of a 2/2 HfN/ScN metal/semiconductor superlattice is presented in figure 1(a)). Since HfN and ScN have similar lattice constants (4.52 Å), all the superlattices are

assumed to grow epitaxially with an in-plane lattice constant of 4.52 Å. Along the cross-plane direction, we see slight reduction in the lattice constant with significant structural relaxation at the metal/semiconductor interface.

The interface energy density (IED) of these superlattices are calculated using the formula

$$[mE_{(\text{bulk-HfN})} + nE_{(\text{bulk-ScN})} - (m+n)E_{(\text{HfN/ScN})}]/a^2$$

where  $E_{(\text{HfN/ScN})}$ ,  $E_{(\text{bulk-HfN})}$ , and  $E_{(\text{bulk-ScN})}$  are the energies of the HfN/ScN superlattice, bulk HfN and bulk ScN respectively, and  $a^2$  is the interface area. Figure 1(b) suggests that the IED converges as we increase the period of the superlattice from 4/4 to 6/6. The IED is also positive, and the values of 0.45–0.5 J m<sup>-2</sup> are typical for a coherent interface with an excess interface free energy contribution that is relatively large as expected for materials with high bond energy, corresponding to the high melting temperature of the component materials (2600 °C and 3305 °C for ScN and HfN respectively). Our calculated interface energy densities for HfN-based superlattices (e.g. 0.49 J m<sup>-2</sup> for a 6/6 superlattice) are higher than those obtained for ZrN-based superlattices [18] (where an IED of 0.29 J m<sup>-2</sup>

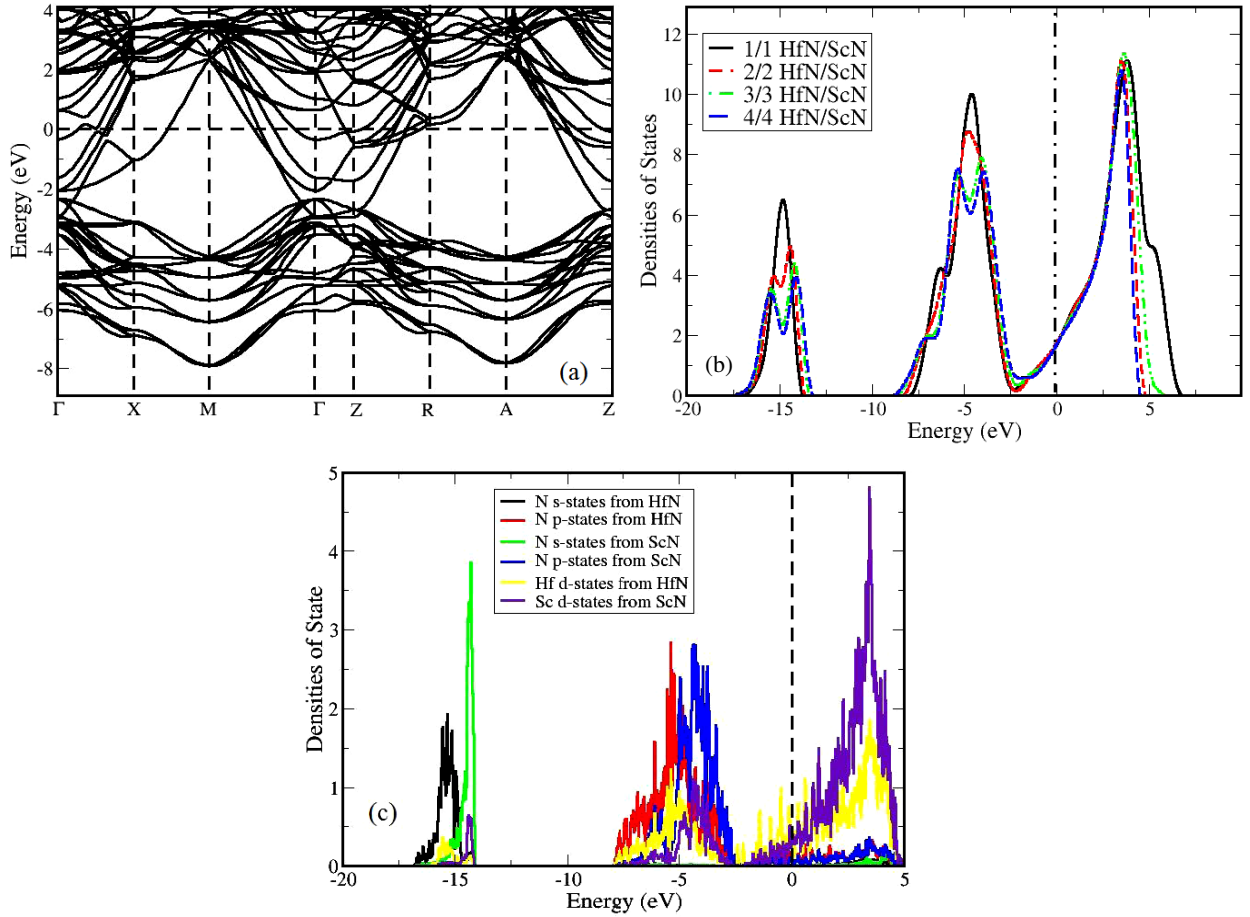


**Figure 2.** (a) Electronic structure of a 2/2 HfN/ScN metal/semiconductor superlattice along the high symmetry directions of the Brillouin zone. The high symmetry points are  $\Gamma(0, 0, 0)$ ,  $X(0, \frac{1}{2}, 0)$ ,  $M(\frac{1}{2}, \frac{1}{2}, 0)$ ,  $Z(0, 0, \frac{1}{2})$ ,  $R(0, \frac{1}{2}, \frac{1}{2})$ , and  $A(\frac{1}{2}, \frac{1}{2}, \frac{1}{2})$ . Electronic bands are seen to be flattening near the Fermi energy along the  $\Gamma$ -Z directions. (b) The normalized electronic density of states of HfN/ScN superlattice with varying periods. Large asymmetry in DOS can be seen near the Fermi energy. (c) Partial densities of electronic state for a typical 2/2 superlattice. Nitrogen s and p-band peaks from the HfN and ScN sides are seen separated.

is estimated for the 6/6 superlattice). Since HfN has a higher melting temperature (3305 °C) and bonding energy than ZrN (2930 °C), the IEDs for HfN-based superlattices are higher.

### 3.2. Electronic structure

To understand the electrical transport properties of HfN/ScN metal/semiconductor superlattices, we have determined the electronic structure of  $m/n$  superlattices with  $m$  and  $n = 1-4$ . The dispersion spectra of the 2/2 superlattice (typical of any other  $m/n$  superlattices) indicates that along the in-plane transport direction (i.e.  $\Gamma$ -X) the superlattices are metallic in nature with the Fermi level inside the conduction band (see figure 2(a)), while along the cross-plane  $\Gamma$ -Z direction, electronic bands flatten out near the Fermi energy. Since flat electronic bands have low curvature and high effective mass, the Seebeck coefficient of these superlattices should be much higher along the cross-plane directions compared to the in-plane  $\Gamma$ -X directions.

Careful observation of figure 2(a) also suggests the presence of doubly degenerate electronic bands that are 0.35 eV and 0.09 eV below the Fermi energy at the  $\Gamma$  and Z

points respectively, representing the superlattice’s degenerate nature. The electronic bands just above the Fermi energy are 0.60 eV and 0.76 eV away from the Fermi energy at the  $\Gamma$  and Z-points respectively. Since the theoretical models of Shakouri *et al* [13, 14] have suggested degenerate semiconductor or metallic superlattices with tall barrier height, HfN/ScN metal/semiconductor superlattices seem to be suitable candidates to achieve high power factors.

The normalized electronic density of states (DOS) (presented in figure 2(b) with different period thicknesses) has a large degree of asymmetry at the Fermi energy, i.e. a much higher density of states at  $E > E_F$  than at  $E < E_F$ . Such asymmetry in the DOS is necessary to achieve a higher power factor according to the Mahan–Sofo Theory [26]. The partial densities of state (PDOS) indicate (see figure 2(c)) that the s and p-states of nitrogen in the superlattice from HfN and ScN span almost the same energy range. However their peak positions are separated by 1.01 eV and 1.04 eV respectively for the s and p bands. In bulk HfN and ScN the nitrogen s and p-state peaks were separated by 3.2 eV, as seen in our earlier work [16]. The extent of the separation of these peak positions suggests the realignment of electronic

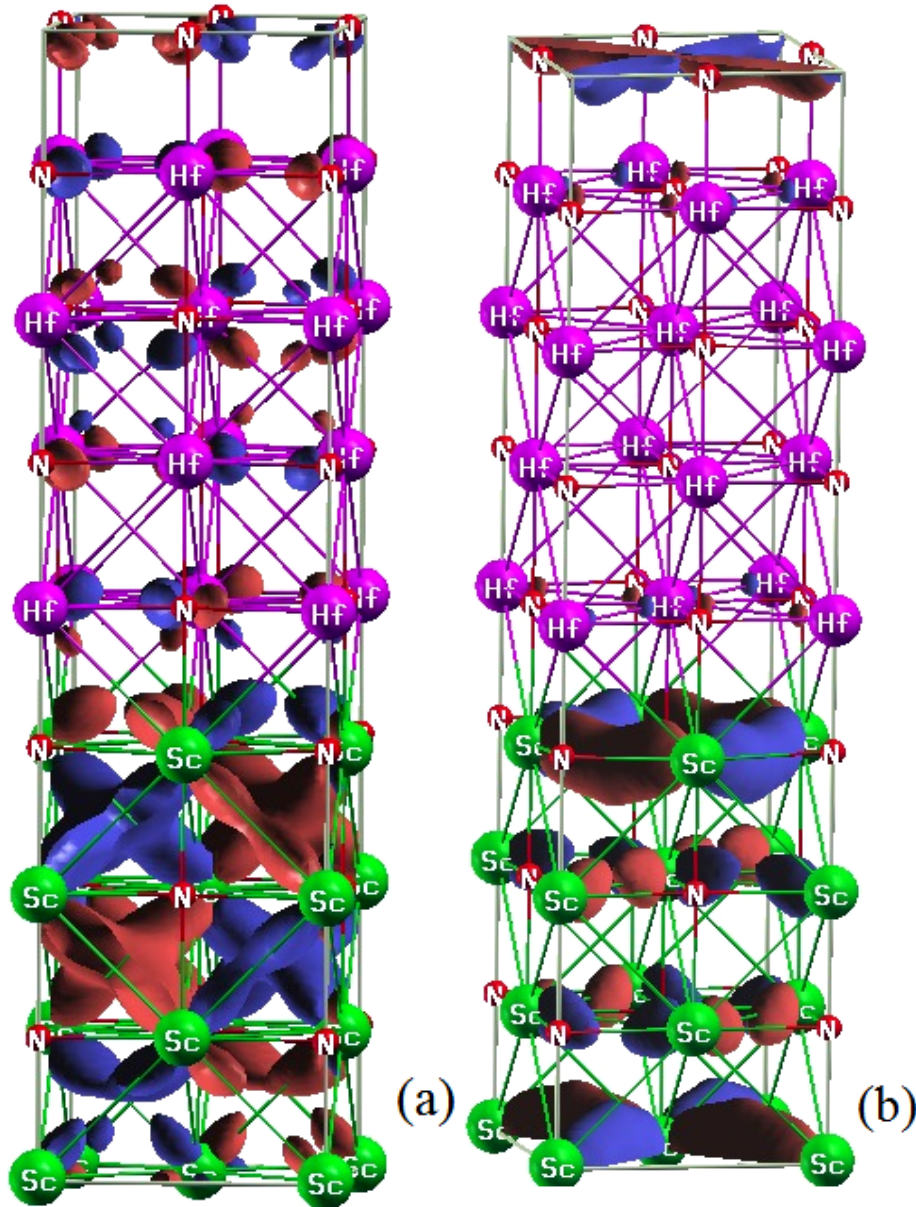


**Figure 3.** (a) Highest occupied and (b) lowest unoccupied electronic states at the  $\Gamma$ -point of the Brillouin zone for a 4/4 HfN/ScN superlattice.

bands when a metal/semiconductor interface is created. The PDOS also indicates that the Fermi energy has moved inside the conduction band of ScN, with the tail of d-states moving almost 2 eV below the Fermi energy.

To understand the nature of electronic states near the Fermi energy responsible for electron transport, we have also visualized (see figures 3(a) and (b)) the highest occupied and lowest unoccupied electronic states at the  $\Gamma$ -point of the Brillouin zone. The highest occupied state at the  $\Gamma$ -point are hybridized d-states of Sc and are largely confined in the ScN layer, while the lowest unoccupied states are mostly Sc d-orbitals and are confined at the metal/semiconductor interface. The cross-plane coupling at the interface is also very minimal, indicating that the current flow across the interface will be very small.

### 3.3. Estimation of Schottky barrier height

The cross-plane electrical transport in the metal/semiconductor superlattices is primarily dominated by the Schottky barrier height. The barrier height is an intrinsic property of the metal and semiconductor interface and arises from the relative positions of the metal's Fermi energy with respect to the semiconductor valence band maximum (for p-type barrier) and to the conduction band minimum (for n-type barriers). The interface chemical bonds and dipoles resulting from the charge transfer at the interface also play crucial roles in the barrier type and overall barrier height. Understanding the barrier formation mechanism and its height estimation from first principles is challenging and requires large-scale supercell calculations [27–29]. Here we determine the Schottky barrier height of the HfN/ScN superlattices using

**Table 1.** Estimation of p-type Schottky barrier height as a function of the stacking period of HfN/ScN superlattices (it is clear that the value of the barrier height converges with the 6/6 and 7/7 superlattices).

$n/n$ -HfN/ScN	$E_F$ (eV)	$E_{VBM}$ (eV)	$\Delta V$ (eV)	$\phi$ (eV)
6/6	10.75	8.81	1.18	0.76
7/7	10.75	8.81	1.17	0.77
8/8	10.75	8.81	1.19	0.75

the macroscopic averaging method [29]. The p-type barrier height is given by the expression

$$\phi_p = E_F - E_{VBM} - \Delta V,$$

where  $\Delta V$  is the change in the average electrostatic potential across the interface (positive if higher on the semiconductor side),  $E_F$  is the metal Fermi level referenced to the average electrostatic potential of the bulk metal, and  $E_{VBM}$  is the valence band maximum referenced to the average electrostatic potential of the bulk semiconductor.

The macroscopic average electrostatic potentials as a function of the perpendicular distance from the interface (001) direction (presented in figure 4(a)) are not very smooth, due to large structural relaxation along the cross-plane directions at the metal/semiconductor interface. In order to converge the band alignment at the metal/semiconductor interface, large supercells containing up to 8 layers of metal and 8 layers of semiconductor are used, and the values of the p-type Schottky barrier height as a function of the layer thicknesses are presented in table 1. As evident from table 1, the values of the barrier height converge as we move from the 6/6 to 7/7 layers of the component materials. Since microscopic averaging is not appropriate for very short period superlattices, we do not generate reliable values of  $\Delta V$  if we go below 5/5 layers of superlattice. Our estimate of the p-type Schottky barrier height for the HfN/ScN metal/semiconductor superlattice is 0.77 eV, larger than the p-type barrier height of 0.34 eV for the ZrN/ScN superlattices. The n-type barrier height is obtained by subtracting the p-type barrier height from the indirect band gap of the semiconductor, and the n-type barrier height of the HfN/ScN superlattices is 0.13 eV. As pointed out earlier, since the electron transport along the cross-plane direction strongly depends on the barrier height and n-type barrier height for this material system, we predict from the barrier height estimations that along the cross-plane direction the HfN/ScN superlattices should be much more metallic than its ZrN counterpart, and an immediate consequence of that should be a lower Seebeck coefficient along the transport direction.

Our analysis also suggests a small amount of charge transfer from the semiconductor to the metallic region at the interface (see figure 4(b)). The extent of charge transfer also decays quickly as we move deep inside the metal or in the semiconductor layers. Due to this charge transfer in the layers, dipoles are formed at the metal/semiconductor interface, which affects the Schottky barrier height; however the microscopic averaging method that we have applied successfully takes care of the effect of charge transfer.

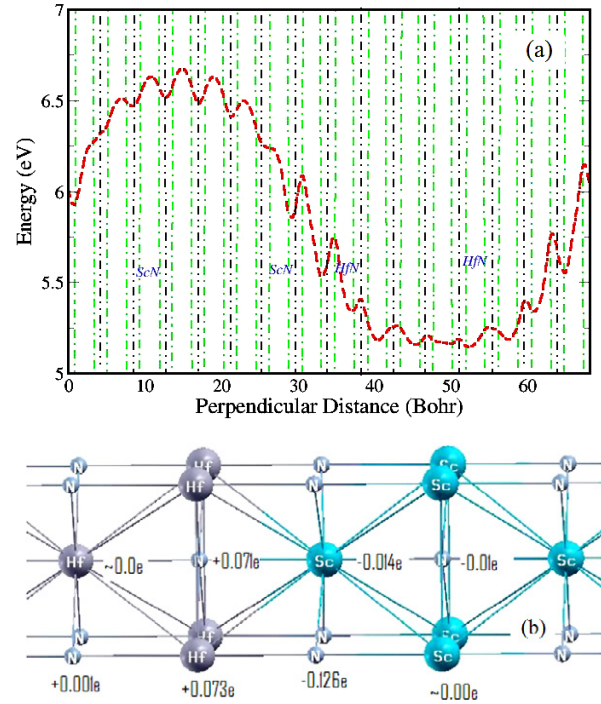


**Figure 4.** (a) Planar average electrostatic potential (oscillating green dashed line) as a function of perpendicular distance from the (001) metal/semiconductor interface. Lattice-plane oscillations are evident, and are filtered with the macroscopic averaging technique (long-dashed red line). Vertical dashed black line represents the lattice planes. The difference of the microscopic average electrostatic potential between metal and semiconductor side is critical for the estimates of the Schottky barrier. (b) Charge transfer from ScN to HfN layers at the interface of 8/8 superlattices. Hf and N atoms on the HfN layer at the interface have gained charge (indicated by the positive sign), whereas Sc and N atoms on ScN layer have lost charge (shown by the negative sign), resulting in the formation of dipoles.

### 3.4. Electrical conductivity and Seebeck coefficients

The calculated electrical conductivity ( $\sigma$ ) of bulk HfN decreases linearly with increasing temperature (see figure 5(a)), representing its metallic character, while we see a normal Arrhenius type temperature variation of electrical conductivity ( $\sigma$ ) in semiconducting ScN (see figure 5(b)). The electrical conductivity of the 2/2 HfN/ScN metal/semiconductor superlattice along the  $\Gamma$ -Z cross-plane direction illustrates metallic behaviour, with  $\sigma$  decreasing linearly with an increase in the temperature, however the value of  $\sigma$  is an order of magnitude smaller than that of bulk HfN. The electrical conductivity of the superlattice is, however, eight orders of magnitude higher than that of stoichiometric bulk ScN. Our results also suggest that the HfN based superlattice has a larger cross-plane electrical conductivity than the equivalent ZrN based superlattices (see [18]), with the 2/2 HfN/ScN superlattice having nearly 100 times greater  $\sigma$  than its 2/2 ZrN counterpart. Metallic-like conduction in the HfN/ScN superlattice is interesting and can be explained through our understanding of the Schottky barrier height estimation presented in section 3.3. The n-type barrier height of 0.13 eV

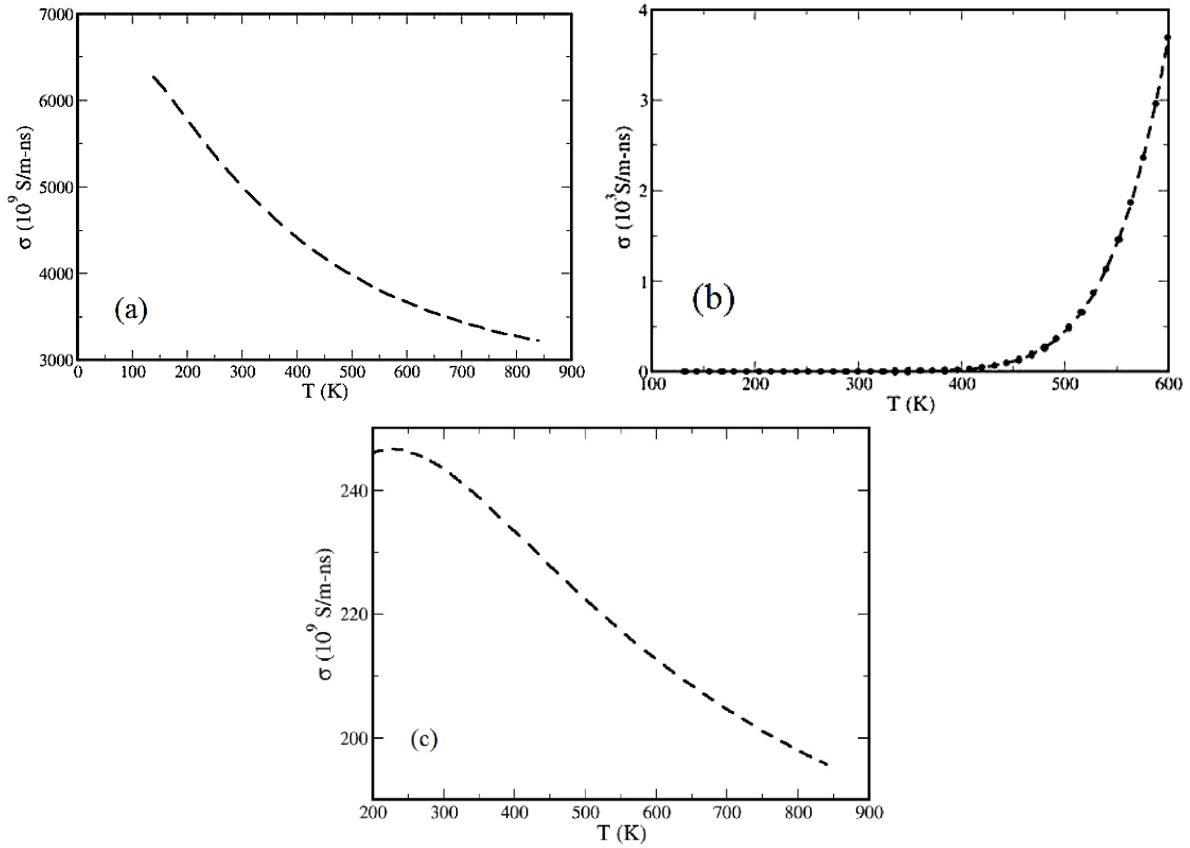


**Figure 5.** Electrical conductivity of (a) HfN (b) ScN (adapted from [18] to compare results), and (c) 2/2 HfN/ScN metal/semiconductor superlattices. While ScN shows normal Arrhenius behaviour in  $\sigma$  versus  $T$ , HfN and the superlattice show metallic type conductivity. Reproduced with permission from [18]. Copyright 2011 American Institute of Physics.

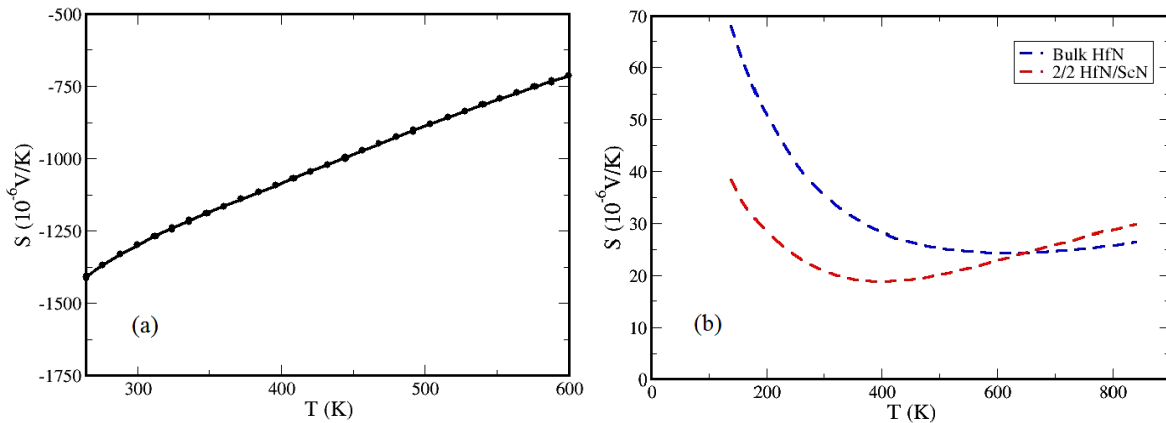


**Figure 6.** Seebeck coefficient of (a) ScN (adapted from [18] to compare results), (b) HfN and 2/2 HfN/ScN superlattices. As can be seen from the figure, the superlattice Seebeck coefficient only exceeds the bulk values at high temperatures. Reproduced with permission from [18]. Copyright 2011 American Institute of Physics.

for the HfN/ScN superlattices is smaller than the ZrN/ScN superlattices, where an n-type barrier height of 0.56 eV is reported [18]. Due to this lower barrier height, electrons can pass through the interface of HfN/ScN superlattices much more easily than the ZrN/ScN superlattices resulting in a higher cross-plane electrical conductivity. Our results are in agreement with the experimental observation [30] of metallic conduction in HfN/ScN metal/semiconductor based superlattices.

We have also estimated the cross-plane Seebeck coefficient of the HfN/ScN superlattices and bulk materials (HfN and ScN; see figure 6). Since we have made a significant approximation of energy-independent and constant relaxation times for all the materials, the reader should concentrate more on the trends in the results than on the absolute values. The Seebeck coefficient ( $S$ ) of bulk ScN is negative (representing its n-type semiconducting behaviour) and decreases in magnitude with increasing temperature above 250 K, while  $S$  of bulk HfN is typical for a metal

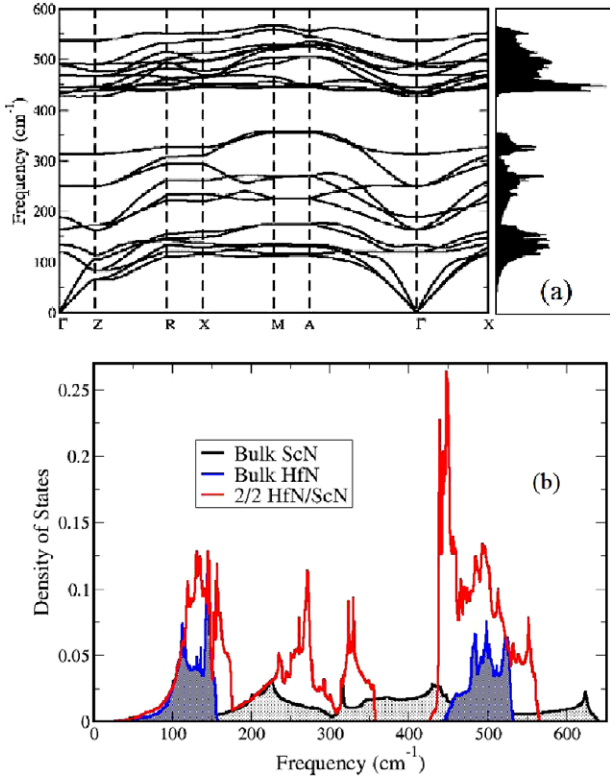


**Figure 7.** Vibrational spectra and density of phonon states of a 2/2 HfN/ScN superlattice along the high-symmetry direction of the tetragonal Brillouin zone. Flat phonon bands are observed along the cross-plane ( $\Gamma$ -Z, R-X, and M-A) directions, representing their localized nature.

and decreases with increasing temperature. The Seebeck coefficient of the 2/2 HfN/ScN superlattice along the  $\Gamma$ -Z direction decreases with increasing temperature up to 400 K, and then increases at higher temperature. The values of the Seebeck coefficient are also smaller compared to the ZrN based superlattices due to the smaller Schottky barrier height.

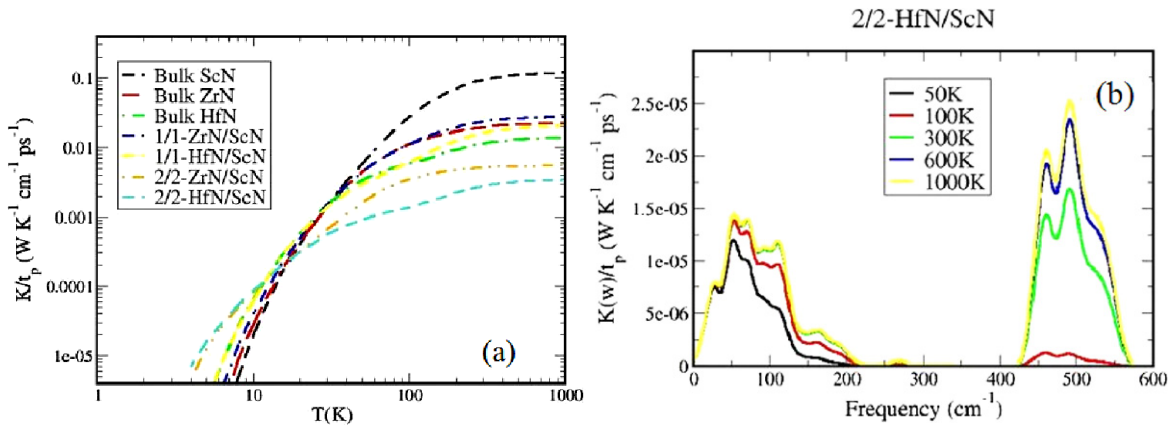


**Figure 8.** (a) Lattice thermal conductivity ( $\kappa$ ) along the cross-plane directions for 1/1 and 2/2 HfN/ScN superlattices.  $\kappa$  of bulk materials and ZrN/ScN superlattices (adapted from our previous work, see [16, 18] respectively) are plotted in the same figure to compare their values. A large reduction of lattice thermal conductivity for HfN-based superlattices is observed compared to component bulk materials and ZrN-based superlattices. (b) Cross-plane lattice thermal conductivity as a function of the phonon frequencies at different temperatures. Reproduced with permission from [18]. Copyright 2011 American Institute of Physics.

Our results reflect the inherent trade-off between the Seebeck coefficient and electrical conductivity, suggesting that it is difficult to simultaneously increase both parameters.

### 3.5. Vibrational spectra and thermal properties

The vibrational spectra of the 2/2 HfN/ScN superlattice suggests (see figure 7(a)) a large reduction in the velocities of the transverse acoustic phonon modes along the cross-plane directions (i.e.  $\Gamma$ -Z, R-X and M-A), while phonon branches along the in-plane directions disperse as steeply as expected from the phonon dispersion of bulk materials. Since bulk HfN and ScN have a large mismatch in the densities of phonon states (large densities of ScN phonon states spanning the frequency range of 160–440  $\text{cm}^{-1}$  where HfN has no states, due to the complete separation of its acoustic and optical phonons (see figure 7(b))), we see localized ScN flat phonon bands in the frequency range of 215–420  $\text{cm}^{-1}$ , making weak contributions to the overall lattice thermal conductivity along the cross-plane direction. The overall localization effect of ScN phonons (i.e. the spread of ScN mini-band between the vibrational energy gap of metal and semiconductor) is larger in HfN-based superlattices compared to ZrN-based superlattices due to the larger mass of Hf compared to Zr [18].

We now analyse the lattice thermal conductivity using Boltzmann transport theory. The scattering or relaxation time, which derives from anharmonic interactions of phonons, is not readily estimated from first principles. Here we assume that the scattering time is constant for all phonons, analyse the cross-plane lattice thermal conductivities of HfN/ScN superlattices with varying periods, and compare them with the component bulk materials as well as ZrN/ScN-based superlattices, which include only the effects of density of states and the group velocity of phonons. Our results indicate a two orders of magnitude reduction in the cross-plane lattice thermal conductivity for the 2/2 superlattice compared to the bulk ScN (see figure 8(a)), while the reduction in  $\kappa$

is by one order of magnitude for the 1/1 superlattices in comparison with bulk HfN. The lattice thermal conductivity of the 1/1 superlattice is between the values for bulk HfN and ScN. In comparison with ZrN/ScN superlattices, the thermal conductivities of HfN-based superlattices are smaller, indicating their relative suitability for thermoelectric applications. These huge reductions in the cross-plane lattice thermal conductivity are due to the phonon filtering effect at the metal/semiconductor interface. The large mismatch in the phonon densities of states of bulk materials prevents the mid-frequency-range optical phonons of ScN from propagating across the interface, thereby reducing the overall lattice thermal conductivity. The primary advantage of using the superlattice structure compared to any degenerate semiconductor for thermoelectric refrigeration and power generation is to reduce the cross-plane lattice thermal conductivity, as pointed out by Venkatasubramanian *et al* [8] for their the high  $ZT$   $\text{Bi}_2\text{Te}_3/\text{Sb}_2\text{Te}_3$  superlattices. Acoustic phonon scattering coupled with the reduction of the velocity of phonons [31] along the cross-plane direction had resulted in the decrease of the thermal conductivity for these superlattices. Thus the 10–100 fold reduction in the cross-plane lattice thermal conductivity of nitride based HfN/ScN superlattices seems ideal for developing highly efficient thermoelectric devices. Figure 8(b) suggests that the optical phonons of the superlattices in the frequency range  $215\text{--}420\text{ cm}^{-1}$  have no contribution to the thermal conductivity due to the phonon filtering at the metal/semiconductor interface. At low temperature, thermal conduction is dominated by the acoustic phonons, while as the temperature is increased optical phonons also start contributing to the  $\kappa$ .

### 3.6. Comparison between HfN/ScN and ZrN/ScN superlattices

Having discussed the thermoelectric properties of HfN/ScN superlattices in the previous sections and ZrN/ScN superlattices in our previous work [18], we now compare these two metal/semiconductor superlattices. In terms of the electronic properties, the primary difference between these two superlattices is the Schottky barrier height, which results in sharp differences in the electrical conductivity and Seebeck coefficient of these two superlattices. While the lower barrier height of 0.13 eV in HfN/ScN superlattices resulted in metallic electrical conductivity and lower Seebeck coefficients, the Seebeck coefficient is much higher for ZrN/ScN superlattices due to their higher barrier height of 0.56 eV. However, with respect to the lattice thermal conductivity HfN/ScN superlattices are proven to be much superior than their ZrN based counterparts. The mid-frequency-range optical phonon filtering in the metal/semiconductor interfaces are much more pronounced in the HfN/ScN superlattices compared to ZrN/ScN, giving an overall 10–100 fold reduction of the lattice thermal conductivity compared to the component bulk materials, and a reduction by a factor of 2–3 with respect to the ZrN/ScN superlattices. Although, no doubt, the ultimate usefulness and effectiveness of these superlattices will be

determined by their experimental analysis, our theoretical calculations are consistent with the observed experimental trends and the presented analysis should help experimentalists to understand these materials better.

### 3.7. Conclusion

In conclusion, we have presented first-principles density functional theory based analysis of the electronic structure, vibrational spectra, and transport properties of HfN/ScN metal/semiconductor superlattices with a motivation to understand their potential and suitability for thermoelectric applications. The electronic structure of these superlattices shows flat conduction bands along the cross-plane directions near the Fermi energy and an asymmetric linearly increasing density of states at the Fermi energy. An n-type Schottky barrier height of 0.13 eV is estimated by the microscopic averaging technique of the electrostatic potential, which suggests that the superlattices are degenerate for electron transport along the cross-plane direction. The cross-plane electrical conductivity estimated within the Boltzmann transport theory shows metallic conduction, which is explained by the barrier height arguments. Vibrational spectra of these superlattices indicate localization of mid-frequency-range ScN optical phonons in the vibrational energy gap between the constituent metal (HfN) and semiconductor (ScN) layers, as a result of which the lattice thermal conductivity along the cross-plane directions is 1–2 orders of magnitude lower than the component bulk materials.

## References

- [1] Snyder G J and Toberer E S 2008 *Nature Mater.* **7** 105–14
- [2] Minnich A J, Dresselhaus M S, Ren Z F and Chen G 2009 *Energy Environ. Sci.* **2** 466–79
- [3] Vineis C J, Shakouri A, Majumdar A and Kanatzidis M G 2010 *Adv. Mater.* **22** 3970–80
- [4] Androulakis J, Lin C H, Kong H J, Uher C, Wu C I, Hogan T, Cook B A, Caillat T, Paraskevopoulos K M and Kanatzidis M G 2007 *J. Am. Chem. Soc.* **129** 9780
- [5] Heremans J P, Jovovic V, Toberer E S, Saramat A, Kurosaki K, Charoenphakdee A, Yamanaka S and Snyder G J 2008 *Science* **321** 554
- [6] Hicks L D and Dresselhaus M S 1993 *Phys. Rev. B* **47** 16631
- [7] Hicks L D and Dresselhaus M S 1993 *Phys. Rev. B* **47** 12727
- [8] Venkatasubramanian R, Siivola E, Colpitts T and O'Quinn B 2001 *Nature* **413** 597
- [9] Harman T C *et al* 2002 *Science* **297** 2229
- [10] Mahan G D 1994 *J. Appl. Phys.* **7** 4362–6
- [11] Mahan G D and Woods L M 1998 *Phys. Rev. Lett.* **80** 4016
- [12] Shakouri A 2005 *IEEE Int. Conf. on Thermoelectrics*
- [13] Vashaee D and Shakouri A 2004 *Phys. Rev. Lett.* **92** 106103
- [14] Vashaee D and Shakouri A 2004 *J. Appl. Phys.* **95** 1233–45
- [15] Zebarzadi M, Bian Z, Singh R, Shakouri A, Wortman R, Rawat V and Sands T D 2009 *J. Electron. Mater.* **38** 960–3
- [16] Saha B, Acharya J, Sands T D and Waghmare U V 2010 *J. Appl. Phys.* **107** 033715
- [17] Saha B, Sands T D and Waghmare U V 2011 *J. Appl. Phys.* **109** 073720
- [18] Saha B, Sands T D and Waghmare U V 2011 *J. Appl. Phys.* **109** 083717
- [19] Rawat V, Kho Y K, Cahill D G and Sands T D 2009 *J. Appl. Phys.* **105** 024909

- [20] Perdew J P, Burke K and Ernzerhof M 1996 *Phys. Rev. Lett.* **77** 3865–8
- [21] Vanderbilt D 1990 *Phys. Rev. B* **41** 7892
- [22] Monkhorst H J and Pack J D 1976 *Phys. Rev. B* **13** 5188
- [23] Methfessel M and Paxton A 1991 *Phys. Rev. B* **40** 3616
- [24] Anisimov V I and Gunnarson O 1991 *Phys. Rev. B* **43** 757
- [25] Baroni S, Gironcoli S D, Corso A D and Giannozzi P 2000 *Rev. Mod. Phys.* **73** 515
- [26] Mahan G and Sofo J O 1996 *Proc. Natl Acad. Sci. USA* **93** 7436
- [27] Tung R T 2001 *Phys. Rev. B* **64** 205310
- [28] Delaney K T, Spaldin N A and Van de Walle C D 2010 *Phys. Rev. B* **81** 165312
- [29] Baldereschi A, Baroni S and Resta R 1988 *Phys. Rev. Lett.* **61** 734
- [30] Schroeder J L, Burmistrova P, Wortman R and Sands T 2012 unpublished
- [31] Wang Y, Liebig C, Xu X and Venkatasubramanian R 2010 *Appl. Phys. Lett.* **97** 083103